Structures and chemical bonding of $B_3O_3^{-/0}$ and $B_3O_3H^{-/0}$: A combined photoelectron spectroscopy and first-principles theory study

Li-Juan Zhao' , Wen-Juan Tian' , Ting Ou, Hong-Guang Xu, Gang Feng, Xi-Ling Xu, Hua-Jin Zhai' , Si-Dian Li' , and Wei-Jun Zheng'

Citation: The Journal of Chemical Physics **144**, 124301 (2016); doi: 10.1063/1.4943768
View online: http://dx.doi.org/10.1063/1.4943768
View Table of Contents: http://aip.scitation.org/toc/jcp/144/12
Published by the American Institute of Physics

Structures and chemical bonding of $B_3O_3^{-/0}$ and $B_3O_3H^{-/0}$: A combined photoelectron spectroscopy and first-principles theory study

Li-Juan Zhao,[1,a)] Wen-Juan Tian,[2,a)] Ting Ou,[2] Hong-Guang Xu,[1] Gang Feng,[1] Xi-Ling Xu,[1] Hua-Jin Zhai,[2,3,b)] Si-Dian Li,[2,b)] and Wei-Jun Zheng[1,b)]

[1]*Beijing National Laboratory for Molecular Sciences, State Key Laboratory of Molecular Reaction Dynamics, Institute of Chemistry, Chinese Academy of Sciences, Beijing 100190, China*

[2]*Nanocluster Laboratory, Institute of Molecular Science, Shanxi University, Taiyuan 030006, China*

[3]*State Key Laboratory of Quantum Optics and Quantum Optics Devices, Shanxi University, Taiyuan 030006, China*

(Received 4 January 2016; accepted 23 February 2016; published online 22 March 2016)

We present a combined photoelectron spectroscopy and first-principles theory study on the structural and electronic properties and chemical bonding of $B_3O_3^{-/0}$ and $B_3O_3H^{-/0}$ clusters. The concerted experimental and theoretical data show that the global-minimum structures of B_3O_3 and B_3O_3H neutrals are very different from those of their anionic counterparts. The $B_3O_3^-$ anion is characterized to possess a V-shaped OB–B–BO chain with overall C_{2v} symmetry (**1A**), in which the central B atom interacts with two equivalent boronyl (B≡O) terminals via B–B single bonds as well as with one O atom via a B=O double bond. The $B_3O_3H^-$ anion has a C_s (**2A**) structure, containing an asymmetric OB–B–OBO zig-zag chain and a terminal H atom interacting with the central B atom. In contrast, the C_{2v} (**1a**) global minimum of B_3O_3 neutral contains a rhombic B_2O_2 ring with one B atom bonded to a BO terminal and that of neutral B_3O_3H (**2a**) is also of C_{2v} symmetry, which is readily constructed from C_{2v} (**1a**) by attaching a H atom to the opposite side of the BO group. The H atom in $B_3O_3H^{-/0}$ (**2A** and **2a**) prefers to interact terminally with a B atom, rather than with O. Chemical bonding analyses reveal a three-center four-electron (3c-4e) π hyperbond in the $B_3O_3H^-$ (**2A**) cluster and a four-center four-electron (4c-4e) π bond (that is, the so-called o-bond) in B_3O_3 (**1a**) and B_3O_3H (**2a**) neutral clusters. © *2016 AIP Publishing LLC.* [http://dx.doi.org/10.1063/1.4943768]

I. INTRODUCTION

Due to the intrinsic electron-deficiency of boron and the large difference of electronegativity between boron and oxygen, boron oxide clusters exhibit exotic bonding characteristics and novel structures.[1] The structural and bonding properties of boron oxide clusters have been explored extensively by experiments[2–11] and theoretical calculations[12–19] in the past decades. In particular, the boronyl (BO) group has a robust triple bond[1–4] and plays an important role in governing the structures and bonding of boronyl chemistry.[20,21] Theoretical calculations showed that the $B_3O_3(BO)_3$ cluster possesses a planar D_{3h} structure and can be considered as a new member of the inorganic benzene family.[22] A recent computational study also suggested that $B_6(BO)_7^-$ can be regarded as a boron oxide analog of $B_6H_7^-$.[17]

Owing to the electron deficiency of the boron element, various multicenter bonds can be formed in boron oxides and boron hydrides. The three-center two-electron (3c-2e) B–H–B bonds were found in diborane over 60 years ago. More recently, theoretical calculations showed that the B–B–B–B/H groups in $B_6(BO)_7^-$ and $B_6H_7^-$ form four-center two-electron (4c-2e) bonds.[17] Dual three-center four-electron (3c-4e) π hyperbonds and rhombic four-center four-electron (4c-4e) π bonds (the o-bond) were also theoretically predicted in the $B_3O_n^{-/0/+}$ (n = 2–4) and $B_4O_4^{-/0}$ clusters.[13,23] Related to boron oxides, hydroboron oxides are important products of high-energy and combustion reactions.[24–26] However, the study on hydroboron oxides at the molecular level has remained very rare, except that the triatomic HBO species has been investigated previously by experiments[27–30] and theoretical calculations.[31,32]

In this work, we investigate the structural and electronic properties and chemical bonding of $B_3O_3^-$ and $B_3O_3H^-$ clusters using anion photoelectron spectroscopy and theoretical calculations. The structures of their neutral counterparts are also studied computationally. It is found that the global-minimum structures of $B_3O_3^-$ and $B_3O_3H^-$ anion clusters are very different from those of their neutral counterparts. Chemical bonding analyses reveal that $B_3O_3H^-$ contains a 3c-4e π hyperbond, while B_3O_3 and B_3O_3H have 4c-4e o-bonds.

II. EXPERIMENTAL AND THEORETICAL METHODS

A. Experimental method

The experiments were carried out on a home-built photoelectron spectroscopy apparatus consisting of a laser vaporization cluster source, a time-of-flight (TOF) mass spec-

a)L.-J. Zhao and W.-J. Tian contributed equally to this work.
b)Authors to whom correspondence should be addressed. Electronic addresses: hj.zhai@sxu.edu.cn; lisidian@sxu.edu.cn; and zhengwj@iccas.ac.cn

trometer, and a magnetic-bottle photoelectron spectrometer, which has been described elsewhere.[33] In brief, the $B_3O_3^-$ and $B_3O_3H^-$ cluster anions were generated by laser ablation of a rotating and translating B_2O_3 disc target with the second harmonic of a nanosecond Nd:YAG laser (Continuum Surelite II-10). Typical laser power used for vaporization was about 10 mJ/pulse in this work. Helium carrier gas with ~4 atm backing pressure was used to cool down the nascent clusters in the source, through supersonic expansion from a pulsed valve (General Valve Series 9). The residual water molecules on the surfaces of the target and laser vaporization source as well as the trace amounts of water molecules in the helium carrier gas were able to provide hydrogen for the formation of $B_3O_3H^-$. The $B_3O_3^-$ and $B_3O_3H^-$ anions were analyzed using the TOF mass spectrometer, mass-selected using a mass gate, decelerated by a momentum decelerator, and photodetached with the beam of another Nd:YAG laser (Continuum Surelite II-10; 532 and 266 nm) or an ArF excimer laser (193 nm). The photoelectrons produced were energy-analyzed using the magnetic-bottle photoelectron spectrometer. The photoelectron spectra were calibrated using the known spectra of Bi^-, Cs^-, Cu^-, and Au^- obtained under similar conditions. The resolution of the photoelectron spectrometer was about 40 meV at an electron kinetic energy of 1 eV.

B. Computational methods

Theoretical calculations were carried out primarily at the density-functional theory (DFT) level. Global-minimum searches for $B_3O_3^{0/-}$ and $B_3O_3H^{0/-}$ clusters were conducted at the DFT level using the Coalescence Kick (CK)[34,35] global-minimum search program, aided with manual structural constructions. The candidate low-lying structures were subsequently optimized using the Becke three parameter hybrid functional combined with Lee-Yang-Parr correlation functional, that is, the B3LYP method.[36,37] The augmented correlation-consistent polarized valence triple-zeta (aug-cc-pVTZ) basis sets were chosen in the calculations.[38,39] Harmonic vibrational frequencies were also calculated at the same level to obtain the zero-point energies and to verify that the reported structures are true minima on the potential energy surfaces.

The ground-state vertical detachment energy (VDE) for an anion cluster was calculated as the energy difference between the neutral and the anion, both at the anionic geometry. The VDEs corresponding to the excited states of a neutral cluster were computed at the time-dependent B3LYP (TD-B3LYP) level.[40,41] The adiabatic detachment energy (ADE) of an anion species was calculated as the energy difference between the neutral and the anion, with the neutral being relaxed to the nearest local minimum using anionic structure as the initial one. To further evaluate the relative energies of the low-lying isomers and to refine the ground-state ADEs and VDEs, single-point calculations were conducted using the more accurate coupled cluster method with single, double, and noniterative triple (CCSD(T)) excitations[42–44] at the optimized B3LYP geometries.

Canonical molecular orbital (CMO) analyses were performed to understand the chemical bonding in these clusters. Natural bond orbital (NBO) analyses were carried out to get the natural atomic charges.[45] All the calculations and analyses were accomplished using the Gaussian 09 software package.[46]

III. EXPERIMENTAL RESULTS

The photoelectron spectra of the $B_3O_3^-$ and $B_3O_3H^-$ anion clusters, recorded at 266 nm and 193 nm photon energies, are shown in Fig. 1. The spectra were taken by mass-selecting the cluster anions of 81 amu, which contain both the $B_3O_3^-$ ($^{11}B_3O_3^-$) and $B_3O_3H^-$ ($^{10}B^{11}B_2O_3H^-$) species due to the existence of two isotopes for boron (^{10}B, 19.9%; ^{11}B, 80.1%). The photoelectron spectra in Fig. 1 thus have the spectral contributions from both $B_3O_3^-$ and $B_3O_3H^-$, as labeled.

The 193 nm spectrum has a broad peak centered at ~1.7 eV, as well as a strong and relatively sharp band centered at 4.20 eV. The former broad peak is attributed to the $B_3O_3H^-$ species, while the latter is assigned to $B_3O_3^-$, which will be discussed in detail later. In the 266 nm spectrum, the peak of $B_3O_3H^-$ is strong and better resolved, whereas that of $B_3O_3^-$ becomes weaker because of the low detection efficiency of the slow electrons. As the low electron binding energy feature of $B_3O_3H^-$ is accessible with the 532 nm photons, the photoelectron spectrum of $B_3O_3H^-$ was also recorded at 532 nm, as shown in Fig. 2. The 532 nm spectrum of $B_3O_3H^-$ was taken by selecting the anion of mass peak 82 amu, which is free from the interference of $B_3O_3^-$. The broad band of $B_3O_3H^-$ (Fig. 1) is much better resolved at 532 nm. Two vibrational modes are tentatively assigned: 0.16 eV (~1290 cm^{-1}) and 0.17 eV (~1370 cm^{-1}).

We can determine the ground-state ADE and VDE of $B_3O_3H^-$ to be 1.50 ± 0.08 and 1.66 ± 0.08 eV, respectively, from the first peak and the highest peak in the vibrationally

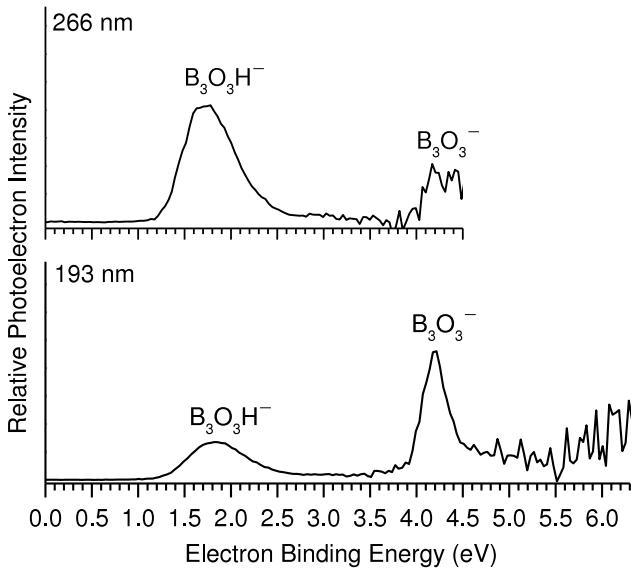

FIG. 1. Photoelectron spectra of the $B_3O_3^-$ and $B_3O_3H^-$ clusters at the 266 and 193 nm photon energies. The peaks contributed by $B_3O_3^-$ and $B_3O_3H^-$ are labeled.

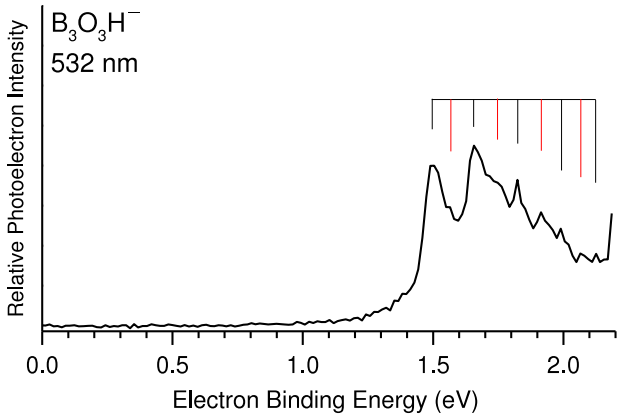

FIG. 2. Photoelectron spectra of the $B_3O_3H^-$ cluster at 532 nm. The vertical lines represent the resolved vibrational structures.

resolved 532 nm spectrum. Specifically, the ADE is evaluated from the vibrational 0–0 transition as resolved at 532 nm (Fig. 2). On the other hand, the ground-state ADE and VDE of $B_3O_3^-$ can be evaluated from the onset and maximum of the second band in the 193 nm spectrum (Fig. 1) to be 3.94 ± 0.08 and 4.20 ± 0.08 eV, respectively. All the experimental ADEs and VDEs are collected in Table I.

IV. THEORETICAL RESULTS

The optimized geometries of the four low-lying isomeric structures of $B_3O_3^-$, $B_3O_3H^-$, and the corresponding neutrals are presented in Fig. 3, along with their relative energies at the single-point CCSD(T)//B3LYP/aug-cc-pVTZ level. The calculated ground-state ADEs and VDEs of low-lying isomers of the $B_3O_3^-$ and $B_3O_3H^-$ anions at both B3LYP/aug-cc-pVTZ and single-point CCSD(T) levels are shown in Table I, where they are compared with the experimental measurements. Furthermore, the photoelectron spectra of the most stable isomers of $B_3O_3^-$ and $B_3O_3H^-$ are simulated on the basis of the B3LYP and TD-B3LYP data and compared with their 193 nm experimental spectrum (Fig. 4). In the simulation, the VDE of the first photoelectron band for a specific species is calculated at the B3LYP level, whereas other peaks associated with the deeper transitions are shifted toward higher binding energies using the excitation energies of its neutral at the corresponding anionic geometry at the TD-B3LYP level. Then all calculated peaks are fitted with unit-area Gaussian functions of 0.1 eV full width at half maximum (FWHM). It is worth mentioning that in some cases there are very large differences between calculated ADEs and VDEs due to the large geometric changes between the anions and neutrals. As the experimental ADEs may not represent the real ADEs due to the possible significant structural changes between the anions and neutrals, we mainly discuss the VDEs in Secs. IV A and IV B.

A. $B_3O_3^-$ and B_3O_3

The global-minimum structure of $B_3O_3^-$ (**1A**; Fig. 3) possesses a V-shaped OB–B–BO chain in which the central B atom interacts with two equivalent boronyl (BO) groups and with one O atom. It has C_{2v} symmetry with an electronic state of $^1A_1$. The calculated ground-state VDE of this structure is 4.12 eV at the single-point CCSD(T) level, in good agreement with the experimental value (4.20 eV; Table I).

The second structure of $B_3O_3^-$ (**1B**) has C_s symmetry and $^1A'$ electronic state. It lies 0.54 eV higher in energy than **1A** at the CCSD(T) level. Similar to **1A**, isomer **1B** also possesses a V-shaped structure, except that one BO group interacts with the central B atom via its O atom instead of B atom. Since **1B** is markedly high in energy, its existence in the cluster beam can be ruled out. Indeed, its calculated first VDE is 4.95 eV, which is much higher than the experimental value (by 0.75 eV).

Additional isomers are more than 1 eV above the **1A** global minimum. Isomer **1C** is 1.24 eV higher in energy. It has a rhombic B_2O_2 four-membered ring and a terminal BO group, the latter interacting with the B_2O_2 ring via a B–B single bond. Its calculated VDE value at the CCSD(T) level is 2.26 eV, deviating drastically from the experimental measurement. Isomer **1D** is 1.31 eV above the global minimum. It has C_{2v} symmetry, which is closely similar in shape to **1A** and **1B**, except that both terminals become the OB groups in **1D**. Here the core B atom is connected to three O atoms. The calculated VDE of **1D** is 5.22 eV, which deviates from the experimental value by 1.02 eV. Overall, isomers **1B**, **1C**, and **1D** can all be

TABLE I. Experimental adiabatic and vertical detachment energies (ADEs and VDEs) of $B_3O_3^-$ and $B_3O_3H^-$ obtained from their photoelectron spectra, as compared with those from theoretical calculations at the B3LYP/aug-cc-pVTZ and single-point CCSD(T)//B3LYP/aug-cc-pVTZ levels. Four isomeric structures are calculated for each anion, and their relative energies (ΔE) are shown. All energies are in eV.

		ΔE	B3LYP		CCSD(T)		Expt.	
Isomers		CCSD(T)	ADE	VDE	ADE	VDE	ADE	VDE
$B_3O_3^-$	**1A**	0.00	3.99	4.06	4.08	4.12	3.94 ± 0.08	4.20 ± 0.08
	1B	0.54	2.64	4.53	2.52	4.95		
	1C	1.24	1.77	2.25	1.82	2.26		
	1D	1.31	4.52	4.54	5.20	5.22		
$B_3O_3H^-$	**2A**	0.00	1.63	1.94	1.44	1.73	1.50 ± 0.08	1.66 ± 0.08
	2B	0.04	0.96	1.25	0.71	0.97		
	2C	0.55	1.66	1.90	1.47	1.67		
	2D	0.62	0.71	3.53	0.82	3.42		

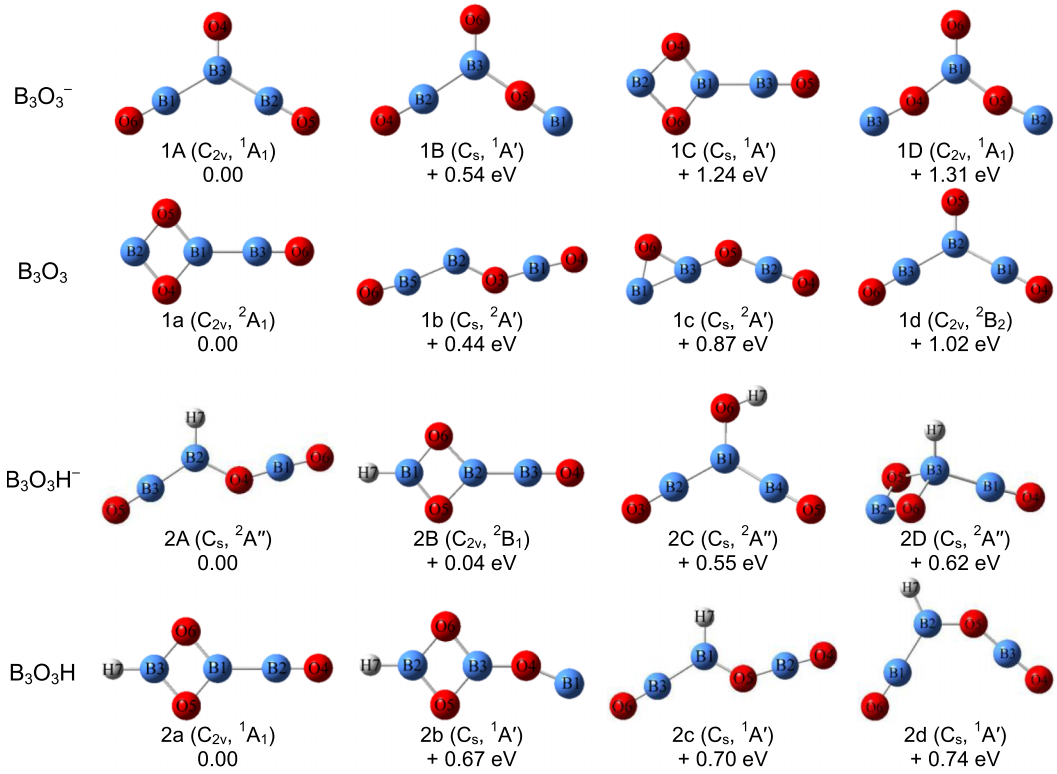

FIG. 3. Typical low-lying isomeric structures of the $B_3O_3^{-/0}$ and $B_3O_3H^{-/0}$ clusters. Their relative energies are shown at the CCSD(T)//B3LYP/aug-cc-pVTZ level.

safely ruled out from experimental observation based on the energetics, which is further confirmed from their calculated first VDEs.

We thus suggest that **1A** is the most probable isomer observed in the experiment. As shown in Fig. 4(b), the simulated spectrum of isomer **1A** is in remarkable agreement with the 193 nm experimental spectrum. Notably, the observed spectral gap in the 4.4–6.3 eV regime is reproduced by **1A**.

It is interesting to note that the global minimum of B_3O_3 neutral (**1a**; Fig. 3) is very different from that of $B_3O_3^-$ anion. Isomer **1a** of neutral B_3O_3 is in fact similar to the third isomer of $B_3O_3^-$ anion (**1C**), with a rhombic B_2O_2 four-membered ring and a terminal BO group. It is a C_{2v} structure, which is slightly higher in symmetry with respect to C_s **1C**. In contrast to $B_3O_3^-$ anion, the V-shaped C_{2v} structure of neutral B_3O_3 (**1d**) is located at 1.02 eV above the global minimum. Thus, a single charge in the system is capable of greatly reversing the relative stabilities of the V-shaped (**1A** and **1d**) versus rhombic (**1C** and **1a**) isomeric structures. We note that global-minimum structures **1A** and **1a** of $B_3O_3^{-/0}$ are consistent with those reported in a recent computational study.[13]

B. $B_3O_3H^-$ and B_3O_3H

The global minimum of $B_3O_3H^-$ (**2A**; Fig. 3) contains an asymmetric OB–B–OBO zig-zag chain, with one BO terminal, one OBO terminal, and a H atom directly bonded with the central B atom. Its symmetry is C_s and its electronic state is $^2A''$. The calculated ground-state VDE of **2A** at the single-point CCSD(T) level is 1.73 eV, in good agreement with the experimental value (1.66 eV; Table I).

Isomer **2B** is marginally higher in energy than **2A** by 0.04 eV; these two structures should be considered isoenergetic in light of the uncertainty of the computational method. Nonetheless, isomer **2B** predicts a first VDE of 0.97 eV, which deviates substantially from the experimental measurement (1.66 eV). Thus, isomer **2B** can be safely ruled out from the experimental observation. Isomer **2B** features a rhombic B_2O_2 four-membered ring with the two B atoms bonded terminally to one H atom and one BO group. Its symmetry is C_{2v} and its electronic state is $^2B_1$. **2B** may be constructed from isomer **1C** of $B_3O_3^-$ (or **1a** of C_{2v} B_3O_3) via the addition of a H terminal.

Isomer **2C** is less stable than **2A** by 0.55 eV, and isomer **2D** is 0.62 eV above the global minimum. Both can be ruled out from the experiment on the basis of the energetics. **2C** has an OH group and two BO groups bonded to the central B atom. **2D** has one B_2O_2 four-membered ring, whose one bridging B atom is bonded with a H atom and one BO group. In short, we suggest isomer **2A** to be the most probable isomer detected in our experiment. The simulated spectrum of isomer **2A** (Fig. 4(c)) is in good agreement with the experimental data at 193 nm, where the calculated VDEs to the excited states of neutral B_3O_3H (**2c**) are 6.07, 6.12, 6.28, and 6.29 eV at the TD-B3LYP level. Interestingly, the simulation shows an extremely large energy gap of ~4.1 eV, indicating remarkable electronic stability of the corresponding neutral B_3O_3H (**2c**) species.

Similar to the case of neutral B_3O_3, the global minimum of neutral B_3O_3 H (**2a**; Fig. 3) turns out to be structurally different from that of $B_3O_3H^-$ anion. Structure **2a** is actually similar to

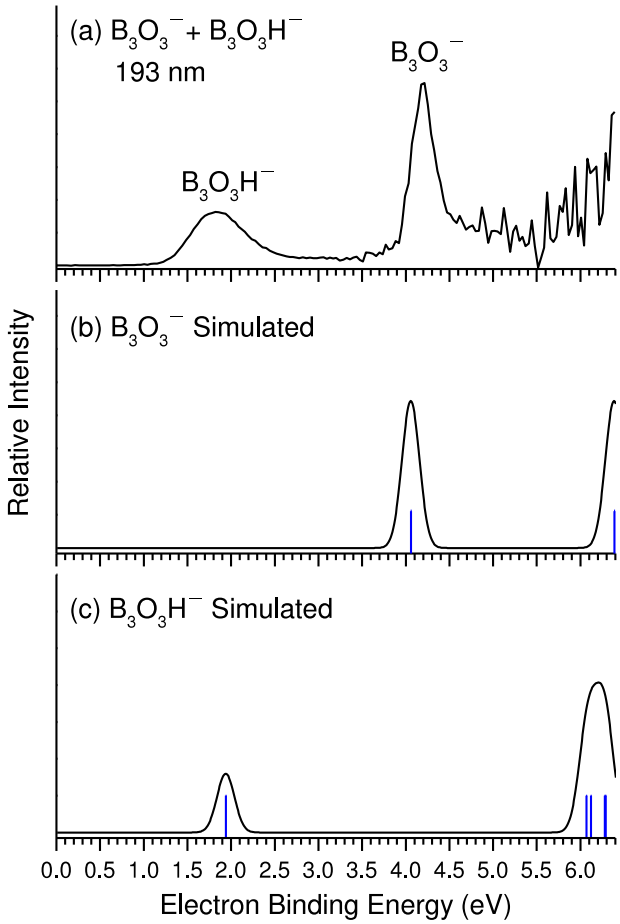

FIG. 4. Comparison between (a) experimental 193 nm photoelectron spectrum and those simulated at the time-dependent B3LYP level on the basis of the most stable isomers of (b) $B_3O_3^-$ and (c) $B_3O_3H^-$. The vertical lines in blue are the calculated vertical detachment energies for $B_3O_3^-$ and $B_3O_3H^-$ clusters.

the second isomer of $B_3O_3H^-$ anion (**2B**), whereas the third isomer of neutral B_3O_3H (**2c**) is relevant to the global minimum of $B_3O_3H^-$ anion (**2A**). The vibrational frequencies of ν_{11} and ν_{12} modes of **2c** are 1149 and 1357 cm^{-1}, respectively, at the B3LYP level. These modes should be responsible for the observed vibrational progressions in the 532 nm spectrum of $B_3O_3H^-$ (1290 and 1370 cm^{-1}; Fig. 2).

V. DISCUSSION

To better understand the chemical bonding and electronic properties of $B_3O_3^-$, $B_3O_3H^-$, and their neutral counterparts, we conducted analyses of the bond distances, natural atomic charges, and CMOs for structures **1A**, **1a**, **2A**, and **2a**. The bond distances and natural atomic charges of $B_3O_3^{-/0}$ and $B_3O_3H^{-/0}$ at the B3LYP/aug-cc-pVTZ level are shown in Fig. 5. Selected key CMOs of interest in $B_3O_3^{-/0}$ and $B_3O_3H^{-/0}$ are presented in Fig. 6. The above analyses allow the proposal of their approximate Lewis presentations, as illustrated in Fig. 7.

A. Bond distances, natural charges, and molecular orbital analyses of $B_3O_3^-$

For the global-minimum structure of $B_3O_3^-$ (**1A**), the bond distances of B4–O1 and B5–O3 are 1.22 Å. These are assigned as B≡O triple bonds because they are close to the boron-oxygen triple bonds (1.21 Å) reported previously.[1,47] The CMOs depicted in Fig. 6 can further confirm the B≡O triple bond characters. The HOMO–8/HOMO–9 pair are readily transformed to two BO σ bonds; whereas the HOMO–4/HOMO–5 and HOMO–3/HOMO–6 pairs constitute four BO π bonds (two for each BO). Collectively, the six CMOs are responsible for B≡O triple bonds for the two BO ligands.

The B6–O2 bond in **1A** is regarded as a B=O double bond, with HOMO–1 constituting its π bond and HOMO–2 its σ bond. The distance of B6–O2 (1.29 Å) is fully consistent with a double bond. The bond distances of B5–B6 and B4–B6 are both 1.74 Å, which can be roughly viewed as B–B single bonds. Note that of the B4/B5/B6 centers, B6 possesses a substantially lower natural charge of +0.10, as

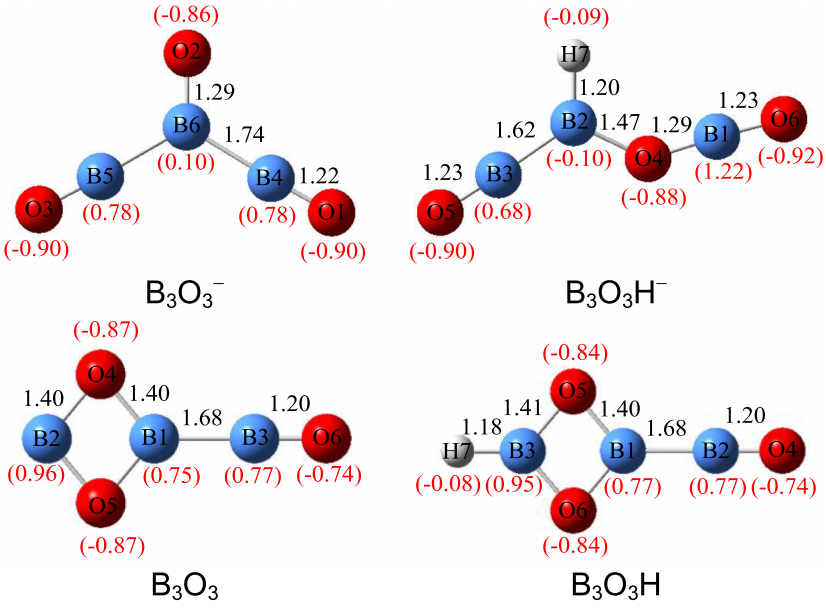

FIG. 5. Calculated bond distances (in Å; in black color) and natural atomic charges (red numbers in the parentheses) of the global-minimum structures of $B_3O_3^-$ (**1A**), B_3O_3 (**1a**), $B_3O_3H^-$ (**2A**), and B_3O_3H (**2a**) at the B3LYP/aug-cc-pVTZ level.

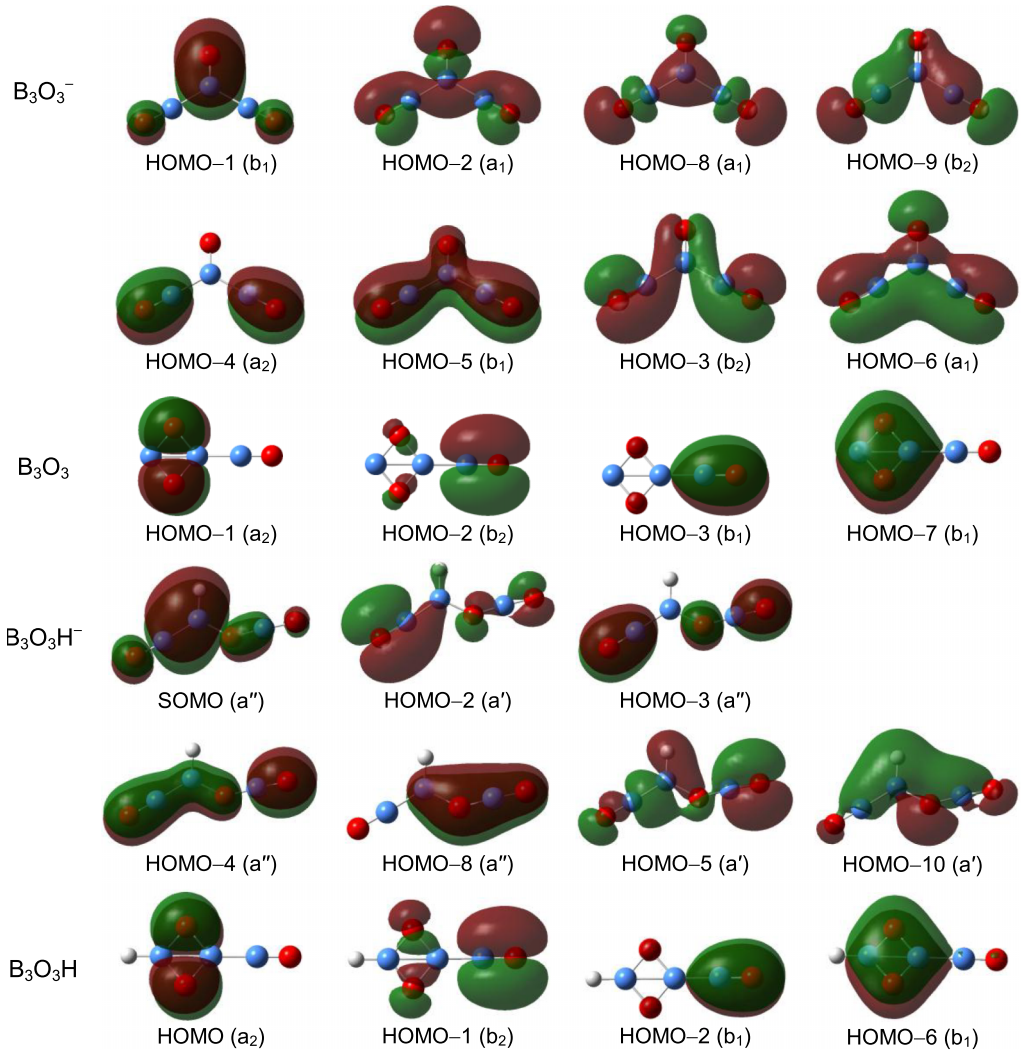

FIG. 6. Selected canonical molecular orbitals (CMOs) of the global-minimum structures of $B_3O_3^-$ (**1A**), B_3O_3 (**1a**), $B_3O_3H^-$ (**2A**), and B_3O_3H (**2a**).

compared to +0.78 for B4/B5, suggesting that the extra charge in $B_3O_3^-$ is largely located on B6. The above bonding pattern of $B_3O_3^-$ (**1A**) can be seen clearly in its Lewis presentation (Fig. 7).

B. On the 3c-4e π hyperbond in $B_3O_3H^-$

The bonding in $B_3O_3H^-$ (**2A**) is more complicated. Thus we do not intend to analyze all relevant CMOs, rather we will show selected ones. The bond distances of B1–O6 and B3–O5 are both 1.23 Å. These BO bonds are assigned to B≡O triple bonds, which can be further confirmed from the CMOs shown in Fig. 6. For example, HOMO–2 and HOMO–3 are π bonding CMOs primarily for the B3≡O5 ligand. The bond distance of B2–O4 is 1.47 Å, typical for a single bond. According to the singly occupied molecular orbital (SOMO), the B2–B3 bond with a distance of 1.62 Å should possess a "half" B–B 2c-1e π bond in addition to a σ bond, suggesting a formal bond order of 1.5. Indeed, this B–B distance appears to be the shortest of all clusters shown in Fig. 5. In addition, the B2–H7 bond (1.20 Å) can be considered as a single bond.

The O4═B1≡O6 structural block possesses a typical 3c-4e π hyperbond.[13,23,48,49] Specifically, the nonbonding/bonding combination of HOMO–4 and HOMO–8 constitutes such a 3c-4e π hyperbond. HOMO–4 is essentially nonbonding between the B1–O4 and B1–O6 segments, with p_z of O4 (9%), p_z of O6 (48%), and p_z of B1 (5%); HOMO–8 is strongly π bonding between the O4/B1/O6 centers, with the p_z atomic orbitals (AOs) of B1 (15%), O4 (69%), and O6 (11%). This 3c-4e hyperbond is similar to the 3c-4e ω-bond in FHF^-, except that the former is of π nature, whereas the latter is in fact a σ bond.[50]

The HOMO–5 and HOMO–10 constitute another set of π bonding CMOs in the O4═B1≡O6 structural block. However, the former is primarily located on the B1–O6 end, consisting of the p_x AOs of O4 (2%), O6 (52%), and B1 (7%); whereas the latter, HOMO–10, is mainly contributed by the p_x AO of O4 (40%), the p_y AO of O6 (3%), and the s- and p-type AOs of B1 (6%), which is located on the B1–O4 end of the block. These two CMOs are thus more localized, in contrast to the full delocalization of HOMO–8. Thus the HOMO–5/HOMO–10 combination is assigned as two 2c-2e π bonds: one for B1–O6 and another for B1–O4.

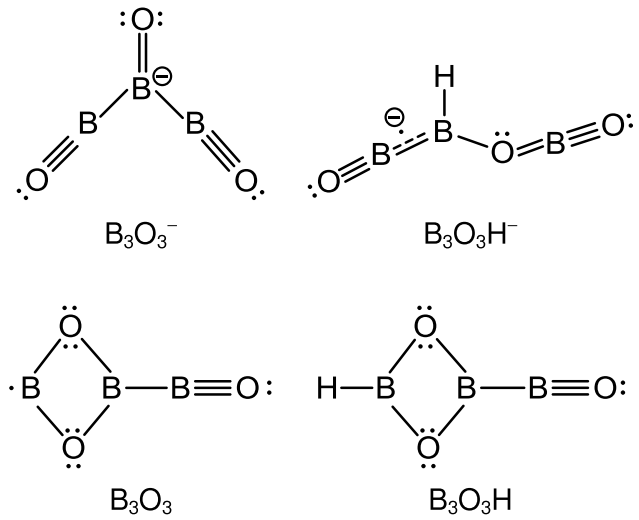

FIG. 7. Schematic Lewis presentations for the global-minimum structures of $B_3O_3^{-/0}$ (**1A** and **1a**) and $B_3O_3H^{-/0}$ (**2A** and **2a**).

In terms of the natural atomic charges, that on the B2 center (−0.10) appears to be markedly lower than those on B3 (+0.68) and B1 (+1.22), indicating that the extra charge in $B_3O_3H^-$ is primarily associated with the B2 center, consistent with the nature of the SOMO in which there is a "half" 2c-1e π bond between B2 and B3 atoms (Fig. 6). Overall, the essence of bonding in $B_3O_3H^-$ (**2A**) is summarized as the approximate Lewis presentation as shown in Fig. 7.

C. Rhombic 4c-4e π bond in B_3O_3 and B_3O_3H

For neutral B_3O_3 (**1a**), the bond distance of B3–O6 is 1.20 Å, which is straightforwardly assigned as a B≡O triple bond. HOMO–2 and HOMO–3 in Fig. 6 constitute the π_y and π_x bonding CMOs of the B3≡O6 bond. The B1–B3 bond (1.68 Å) between the BO group and B_2O_2 four-membered ring is a typical single bond. The bond distances of four B–O bonds within the four-membered B_2O_2 ring are all 1.40 Å. These are roughly considered as single B–O bonds.

An analysis of the CMOs shows that the rhombic B_2O_2 unit in **1a** features a 4c-4e o-bond,[13,23,51] which is contributed by the nonbonding/bonding combination of HOMO–1 and HOMO–7 (Fig. 6). HOMO–1 is composed of the p_x AOs of the two relevant O atoms, which is essentially nonbonding. On the other hand, HOMO–7 is a strongly delocalized, completely bonding π_x CMO. The HOMO–1/HOMO–7 4c-4e o-bond makes use of four electrons from the two O centers, which would otherwise be two O 2p lone-pairs, for one completely bonding 4c-2e π bond as well as one "residual" nonbonding CMO. This bonding effect helps stabilize the electron-deficient boron oxide systems.

It is stressed that the 4c-4e o-bond should not be confused with a typical 4π antiaromatic system, in which the two π CMOs are in an antibonding/bonding combination. The 4c-4e o-bond system is considered to be π aromatic, because the two nonbonding electrons do not contribute to either bonding or antibonding and should be neglected in electron counting in the $(4n + 2)$ or $4n$ Hückel rules. The Lewis presentation of B_3O_3 (**1a**) is shown in Fig. 7.

For neutral B_3O_3H (**2a**), all bond distances and natural atomic charges are virtually identical to those in B_3O_3 (**1a**), except that the former has one extra B–H terminal. Indeed, the B2 center in **1a** is a radical (Fig. 7), which can readily form a σ bond with H to produce **2a**. The B3–H7 terminal in **2a** has a distance of 1.18 Å and is assigned to a single bond, similar to that in $B_3O_3H^-$ (**2A**). Not surprisingly, B_3O_3H (**2a**) also features a 4c-4e o-bond, being contributed by the nonbonding/bonding combination of HOMO and HOMO–6 (Fig. 6). The Lewis presentation of B_3O_3H (**2a**) is also shown in Fig. 7.

VI. CONCLUSIONS

In conclusion, we have investigated the electronic, structural, and bonding properties of the $B_3O_3^-$ and $B_3O_3H^-$ clusters, as well as their neutrals, using a combination of photoelectron spectroscopy and theoretical calculations. The experimental vertical detachment energies of $B_3O_3^-$ and $B_3O_3H^-$ differ markedly, being measured to be 4.20 ± 0.08 and 1.66 ± 0.08 eV, respectively. The global-minimum structures of $B_3O_3^-$, $B_3O_3H^-$, and their neutrals are identified through computational structural searches and electronic structure calculations at the B3LYP and CCSD(T) levels. It is found that $B_3O_3^-$ (**1A**) adopts a V-shaped structure, in which a B═O core interacts with two equivalent B≡O groups via B–B single bonds. $B_3O_3H^-$ (**2A**) contains an asymmetric OB–B–OBO zig-zag chain, where the central B atom has two singly bonded terminals (OBO and H) as well as one terminal BO with the formal bond order of 1.5. In contrast, their neutral species (**1a** and **2a**) each possess a rhombic B_2O_2 ring, one of whose B centers is bonded with a B≡O unit to generate B_3O_3 (**1a**). By adding a H atom to B_3O_3 (**1a**) via a terminal B–H bond, one further reaches B_3O_3H (**2a**). Note that the anionic structures **1A** and **2A** are very different from those of their neutral counterparts (**1a** and **2a**). Chemical bonding analyses reveal a 3c-4e π hyperbond in $B_3O_3H^-$ (**2A**) and rhombic 4c-4e o-bonds in both B_3O_3 (**1a**) and B_3O_3H (**2a**). Approximate Lewis structures are also presented for $B_3O_3^{-/0}$ (**1A** and **1a**) and $B_3O_3H^{-/0}$ (**2A** and **2a**).

ACKNOWLEDGMENTS

This work was supported by the National Natural Science Foundation of China (Nos. 21243004, 21373130, 21273246, and 21573138), the Shanxi International Cooperation project (No. 2013081018), and the State Key Laboratory of Quantum Optics and Quantum Optics Devices (No. KF201402). H.J.Z. gratefully acknowledges the start-up fund from Shanxi University for support.

[1]H.-J. Zhai, Q. Chen, H. Bai, S.-D. Li, and L.-S. Wang, Acc. Chem. Res. **47**, 2435 (2014).
[2]P. G. Wenthold, J. B. Kim, K.-L. Jonas, and W. C. Lineberger, J. Phys. Chem. A **101**, 4472 (1997).
[3]H.-J. Zhai, S.-D. Li, and L.-S. Wang, J. Am. Chem. Soc. **129**, 9254 (2007).
[4]S.-D. Li, H.-J. Zhai, and L.-S. Wang, J. Am. Chem. Soc. **130**, 2573 (2008).
[5]H.-J. Zhai, L.-M. Wang, S.-D. Li, and L.-S. Wang, J. Phys. Chem. A **111**, 1030 (2007).

[6]J. Nicholas, S. Sinogeikin, J. Kieffer, and J. Bass, Phys. Rev. Lett. **92**, 215701 (2004).
[7]H.-J. Zhai, J.-C. Guo, S.-D. Li, and L.-S. Wang, ChemPhysChem **12**, 2549 (2011).
[8]Q. Chen, H.-J. Zhai, S.-D. Li, and L.-S. Wang, J. Chem. Phys. **137**, 044307 (2012).
[9]Q. Chen, H. Bai, H.-J. Zhai, S.-D. Li, and L.-S. Wang, J. Chem. Phys. **139**, 044308 (2013).
[10]W.-J. Tian, H.-G. Xu, X.-Y. Kong, Q. Chen, W.-J. Zheng, H.-J. Zhai, and S.-D. Li, Phys. Chem. Chem. Phys. **16**, 5129 (2014).
[11]H.-J. Zhai, C.-Q. Miao, S.-D. Li, and L.-S. Wang, J. Phys. Chem. A **114**, 12155 (2010).
[12]G. Ferlat, T. Charpentier, A. P. Seitsonen, A. Takada, M. Lazzeri, L. Cormier, G. Calas, and F. Mauri, Phys. Rev. Lett. **101**, 065504 (2008).
[13]Q. Chen, H. Lu, H.-J. Zhai, and S.-D. Li, Phys. Chem. Chem. Phys. **16**, 7274 (2014).
[14]M. T. Nguyen, M. H. Matus, V. T. Ngan, D. J. Grant, and D. A. Dixon, J. Phys. Chem. A **113**, 4895 (2009).
[15]T. B. Tai and M. T. Nguyen, Chem. Phys. Lett. **483**, 35 (2009).
[16]T. B. Tai, M. T. Nguyen, and D. A. Dixon, J. Phys. Chem. A **114**, 2893 (2010).
[17]J.-C. Guo, H.-G. Lu, H.-J. Zhai, and S.-D. Li, J. Phys. Chem. A **117**, 11587 (2013).
[18]X.-J. Feng, Y.-H. Luo, X. Liang, L.-X. Zhao, and T.-T. Cao, J. Cluster Sci. **19**, 421 (2008).
[19]M. L. Drummond, V. Meunier, and B. G. Sumpter, J. Phys. Chem. A **111**, 6539 (2007).
[20]H. Bock, L. Cederbaum, W. von Niessen, P. Paetzold, P. Rosmus, and B. Solouki, Angew. Chem., Int. Ed. Engl. **28**, 88 (1989).
[21]H. Bock, L. S. Cederbaum, W. von Niessen, P. Paetzold, P. Rosmus, and B. Solouki, Angew. Chem. **101**, 77 (1989).
[22]D.-Z. Li, H. Bai, Q. Chen, H. Lu, H.-J. Zhai, and S.-D. Li, J. Chem. Phys. **138**, 244304 (2013).
[23]W.-J. Tian, L.-J. Zhao, Q. Chen, T. Ou, H.-G. Xu, W.-J. Zheng, H.-J. Zhai, and S.-D. Li, J. Chem. Phys. **142**, 134305 (2015).
[24]R. F. Porter and W. P. Sholette, J. Chem. Phys. **37**, 198 (1962).
[25]W. P. Sholette and R. F. Porter, J. Phys. Chem. **67**, 177 (1963).
[26]L. Barton, F. A. Grimm, and R. F. Porter, Inorg. Chem. **5**, 2076 (1966).
[27]E. R. Lory and R. F. Porter, J. Am. Chem. Soc. **93**, 6301 (1971).
[28]Y. Kawashima, K. Kawaguchi, and E. Hirota, Chem. Phys. Lett. **131**, 205 (1986).
[29]Y. Kawashima, Y. Endo, K. Kawaguchi, and E. Hirota, Chem. Phys. Lett. **135**, 441 (1987).
[30]Y. Kawashima, Y. Endo, and E. Hirota, J. Mol. Spectrosc. **133**, 116 (1989).
[31]M. Sobczyk, I. Anusiewicz, P. Skurski, and J. Simons, Mol. Phys. **101**, 1259 (2003).
[32]N. J. DeYonker, S. Li, Y. Yamaguchi, H. F. Schaefer, T. D. Crawford, R. A. King, and K. A. Peterson, J. Chem. Phys. **122**, 234316 (2005).
[33]H.-G. Xu, Z.-G. Zhang, Y. Feng, J. Yuan, Y. Zhao, and W. Zheng, Chem. Phys. Lett. **487**, 204 (2010).
[34]A. P. Sergeeva, B. B. Averkiev, H.-J. Zhai, A. I. Boldyrev, and L.-S. Wang, J. Chem. Phys. **134**, 224304 (2011).
[35]M. Saunders, J. Comput. Chem. **25**, 621 (2004).
[36]C. Lee, W. Yang, and R. G. Parr, Phys. Rev. B **37**, 785 (1988).
[37]A. D. Becke, J. Chem. Phys. **98**, 5648 (1993).
[38]R. A. Kendall, T. H. Dunning, and R. J. Harrison, J. Chem. Phys. **96**, 6796 (1992).
[39]K. A. Peterson, D. Figgen, E. Goll, H. Stoll, and M. Dolg, J. Chem. Phys. **119**, 11113 (2003).
[40]M. E. Casida, C. Jamorski, K. C. Casida, and D. R. Salahub, J. Chem. Phys. **108**, 4439 (1998).
[41]R. Bauernschmitt and R. Ahlrichs, Chem. Phys. Lett. **256**, 454 (1996).
[42]G. E. Scuseria and H. F. Schaefer, J. Chem. Phys. **90**, 3700 (1989).
[43]R. J. Bartlett and M. Musiał, Rev. Mod. Phys. **79**, 291 (2007).
[44]J. Čížek, *Advance Chemical Physics* (John Wiley & Sons Inc., 2007), p. 35.
[45]E. D. Glendening, J. K. Badenhoop, A. E. Reed, J. E. Carpenter, J. A. Bohmann, C. M. Morales, and F. Weinhold, *NBO 5.0* (Theoretical Chemistry Institute, University of Wisconsin, Madison, 2001).
[46]M. J. Frisch, G. W. Trucks, H. B. Schlegel, G. E. Scuseria, M. A. Robb, J. R. Cheeseman, G. Scalmani, V. Barone, B. Mennucci, G. A. Petersson, H. Nakatsuji, M. Caricato, X. Li, H. P. Hratchian, A. F. Izmaylov, J. Bloino, G. Zheng, J. L. Sonnenberg, M. Hada, M. Ehara, K. Toyota, R. Fukuda, J. Hasegawa, M. Ishida, T. Nakajima, Y. Honda, O. Kitao, H. Nakai, T. Vreven, J. A. Montgomery, Jr., J. E. Peralta, F. Ogliaro, M. J. Bearpark, J. Heyd, E. N. Brothers, K. N. Kudin, V. N. Staroverov, R. Kobayashi, J. Normand, K. Raghavachari, A. P. Rendell, J. C. Burant, S. S. Iyengar, J. Tomasi, M. Cossi, N. Rega, N. J. Millam, M. Klene, J. E. Knox, J. B. Cross, V. Bakken, C. Adamo, J. Jaramillo, R. Gomperts, R. E. Stratmann, O. Yazyev, A. J. Austin, R. Cammi, C. Pomelli, J. W. Ochterski, R. L. Martin, K. Morokuma, V. G. Zakrzewski, G. A. Voth, P. Salvador, J. J. Dannenberg, S. Dapprich, A. D. Daniels, Ö Farkas, J. B. Foresman, J. V. Ortiz, J. Cioslowski, and D. J. Fox, GAUSSIAN 09, Revision D.01, Gaussian, Inc., Wallingford, CT, USA, 2009.
[47]H. Braunschweig, K. Radacki, and A. Schneider, Science **328**, 345 (2010).
[48]W.-J. Tian, X.-R. You, D.-Z. Li, T. Ou, Q. Chen, H.-J. Zhai, and S.-D. Li, J. Chem. Phys. **143**, 064303 (2015).
[49]T. Ou, W.-J. Tian, X.-R. You, Y.-J. Wang, K. Wang, and H.-J. Zhai, Phys. Chem. Chem. Phys. **17**, 29697 (2015).
[50]F. Weinhold and C. R. Landis, *Valency and Bonding: A Natural Bond Orbital Donor-Acceptor Perspective* (Cambridge University Press, Cambridge, 2005).
[51]D.-Z. Li, L.-J. Zhang, T. Ou, H.-X. Zhang, L. Pei, H.-J. Zhai, and S.-D. Li, Phys. Chem. Chem. Phys. **17**, 16798 (2015).